

Ground state and magnetic phase transitions of orthoferrite DyFeO₃

Z. Y. Zhao,¹ X. Zhao,^{2,*} H. D. Zhou,^{3,4} F. B. Zhang,¹ Q. J. Li,^{1,5} C. Fan,¹ X. F. Sun,^{1,†} and X. G. Li^{1,6}

¹*Hefei National Laboratory for Physical Sciences at Microscale,
University of Science and Technology of China, Hefei, Anhui 230026, People's Republic of China*

²*School of Physical Sciences, University of Science and Technology of China,
Hefei, Anhui 230026, People's Republic of China*

³*Department of Physics and Astronomy, University of Tennessee, Knoxville, Tennessee 37996-1200, USA*

⁴*National High Magnetic Field Laboratory, Florida State University, Tallahassee, Florida 32306-4005, USA*

⁵*School of Physics and Material Science, Anhui University,
Hefei, Anhui 230039, People's Republic of China*

⁶*Department of Physics, University of Science and Technology of China,
Hefei, Anhui 230026, People's Republic of China*

(Dated: July 11, 2018)

Low-temperature thermal conductivity (κ), as well as magnetization (M) and electric polarization (P), of multiferroic orthoferrite DyFeO₃ single crystals are studied with $H \parallel c$. When the crystal is cooled in zero field, M , P , and κ all consistently exhibit irreversible magnetic-field dependencies. In particular, with 500 mK $< T \leq 2$ K, all these properties show two transitions at the first run of increasing field but only the higher-field transition is present in the subsequent field sweepings. Moreover, the ultra-low- T ($T < 500$ mK) $\kappa(H)$ shows a different irreversibility and there is only one transition when the field is swept both up and down. All the results indicate a complex low- T H - T phase diagram involving successive magnetic phase transitions of the Fe³⁺ spins. In particular, the ground state, obtained with cooling to subKelvin temperatures in zero field, is found to be an unexplored phase.

PACS numbers: 75.85.+t, 66.70.-f

I. INTRODUCTION

Magnetic phase transition induced by magnetic field is an outstanding phenomenon in the strongly-correlated electron systems and is associated with many physical interests, such as the unconventional superconductivity,^{1,2} the non-Fermi-liquid behaviors,³ and the multiferroicity,⁴ etc. Multiferroicity induced by spin order has attracted much attention due to its large magnetoelectric (ME) coupling. The spin-current model or the inverse Dzyaloshinsky-Moriya (DM) interaction⁵ can explain well the production of electric polarization (P) in the non-collinear spin systems, such as the perovskite $RMnO_3$ (R = rare earth).^{4,6,7} When the spins are aligned collinearly, P can also be formed through the exchange striction mechanism, such as in $RFeO_3$,⁸⁻¹⁰ Ca_3CoMnO_6 ,¹¹ and RMn_2O_5 .¹²⁻¹⁴ In these materials, the spin structures are playing a key role in the ME coupling and the formation of the spontaneous electric polarization. The rare-earth-based orthoferrites $RFeO_3$ have received a lot of research interests in last several decades, particularly in the manifestations of the spin structures and spin re-orientations.¹⁵⁻¹⁹

In DyFeO₃, the Fe³⁺ moments exhibit $G_x A_y F_z$ (Fe_I) spin configuration in Bertaut's notation²⁰ at room temperature, that is, the main component of the magnetic moment is along the a axis, accompanying with weak ferromagnetism (WFM) along the c axis.^{21,22} Upon lowering temperature, the Fe³⁺ spins undergo a Morin transition²³ at $T_M = 50$ K. At this transition the spin configuration changes to $A_x G_y C_z$ (Fe_{II}).²² Moreover, with an applied

magnetic field, $H > H_r^{Fe}$, along the c axis the Fe³⁺ spin configuration could change back to Fe_I.^{8,24} With further lowering temperature, the Dy³⁺ spins develop a long-range antiferromagnetic (AF) order below $T_N^{Dy} = 4.2$ K.⁸ In the AF state, Dy³⁺ spins are confined in the ab plane and the spin configuration can be expressed as $G_x A_y$ with the Ising axis deviating about 33° from the b axis.^{25,26} The spin-induced multiferroicity was observed only at $T < T_N^{Dy}$ and when the spin flop of Fe³⁺ moments is introduced by a c -axis field.⁸ Due to the interaction between Dy³⁺ and Fe³⁺ spins, the Dy³⁺ spins shift towards the layers of Fe³⁺ with opposite spin directions and far away from those with the same spin directions, resulting in a collective displacement of the Dy³⁺ ions and producing a spontaneous P . Therefore, both the Dy³⁺ and Fe³⁺ spin structures are crucial for the ME phenomenon. However, the spin structure of Fe³⁺ at low temperatures actually has not been determined. An obvious inconsistency in the early studies is that the Mossbauer spectroscopy suggested a $G_x G_y$ structure,²⁷ while the electric polarization results suggested a $A_x G_y C_z$ structure.⁸ Moreover, the ground state and the low- T magnetic phase transitions are actually not known since all the previous works had not studied the physics of DyFeO₃ at temperatures lower than 1.5 K.

Heat transport has been proved to be a useful probe for the low- T magnetic transitions.²⁸⁻³⁵ In this work, we study the low- T thermal conductivity (κ), as well as the magnetization (M) and electric polarization, of DyFeO₃ single crystals with $H \parallel c$ after a zero field cooling (ZFC) process. In particular, the P measurements can be done

at temperatures below 1 K, while the κ is measured at temperatures down to several tens of milli-Kelvin. It is found that $M(H)$, $P(H)$, and $\kappa(H)$ all consistently exhibit peculiar low-field irreversible behaviors at $T > 500$ mK with the irreversibility field smaller than H_r^{Fe} . At $T < 500$ mK, $\kappa(H)$ shows a different irreversibility with larger κ in the field-up process, which is in contrast with the case above 500 mK. The results suggest a complex low- T $H - T$ phase diagram involving successive field-induced magnetic phase transitions of Fe^{3+} spins.

II. EXPERIMENTS

High-quality DyFeO_3 single crystals were grown by a floating-zone technique in flowing oxygen-argon mixture with the ratio of 1:4. The crystals were cut precisely along the crystallographic axes after orientation by using back-reflection x-ray Laue photographs. The sample for magnetization measurement is rod-like and the dimension is $1.70 \times 0.75 \times 0.55 \text{ mm}^3$ with the length, width and thickness along the b , c , and a axis, respectively. The sample for electric polarization measurement is plate-like and the wide face is perpendicular to the c axis with dimension of $2.06 \times 2.14 \times 0.13 \text{ mm}^3$. The dimension of the sample for thermal conductivity measurement is $3.86 \times 0.63 \times 0.14 \text{ mm}^3$ and the longest dimension is parallel to the c axis.

Magnetization was measured by a SQUID-VSM (Quantum Design). Electric polarization was obtained by integrating the displacement current measured by an electrometer (model 6517B, Keithley) in a ^3He refrigerator and a 14 T magnet. $P(T)$ was measured at a rate of about 2 K/min from 300 mK to 5 K. In order to stabilize temperature in the $P(H)$ measurements, the sweeping-field rate must be slower for lower temperature, which is 0.25, 0.2, 0.15, and 0.1 T/min at 2, 1.4, 1, and 0.7 K, respectively. Thermal conductivity was measured by using a “one heater, two thermometers” technique and three different cryostats:^{30–36} (i) in a ^3He - ^4He dilution refrigerator at temperature regime of 70 mK–1 K; (ii) in a ^3He refrigerator at 0.3–8 K, and (iii) in a pulse-tube refrigerator for zero-field data at $T > 5$ K. In all these measurements, the magnetic fields were applied along the c axis.

III. RESULTS AND DISCUSSION

A. Magnetization

The basic magnetic properties of DyFeO_3 are characterized by the $M(T)$ and $M(H)$ measurements, of which the representative data are shown in Fig. 1. These results are in good consistency with the earlier works.^{8,22} The temperature dependence of M along the c axis measured in $H = 500$ Oe, shown in Fig. 1(a), has two transitions at 50 and 4.2 K. The AF order of Fe^{3+} spins is known to

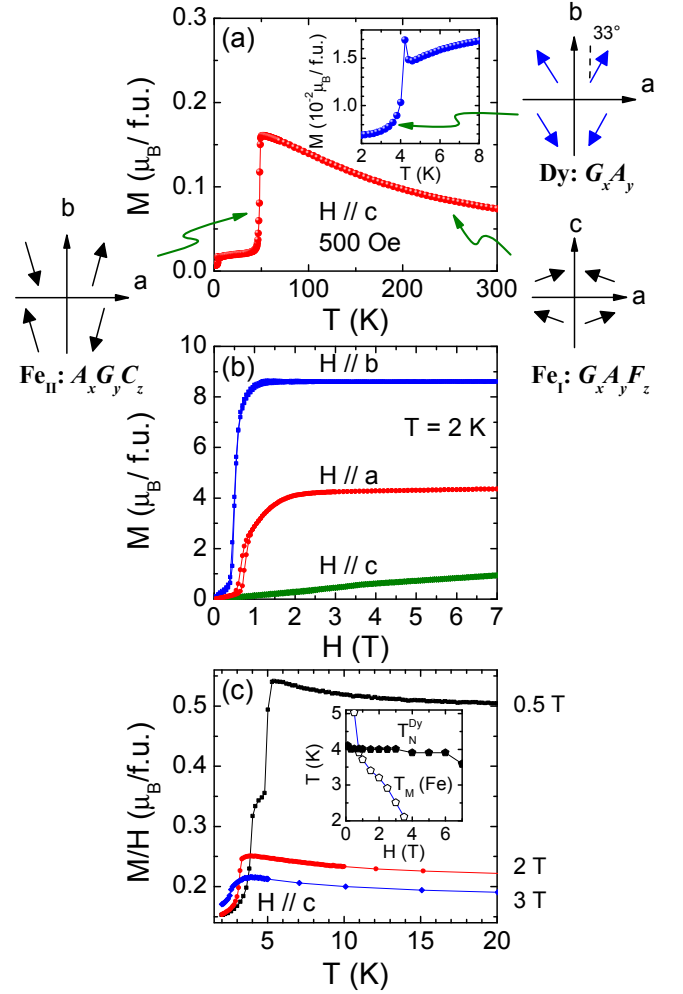


FIG. 1: (Color online) Magnetic properties of DyFeO_3 single crystal. (a) Magnetic susceptibility in $H = 500$ Oe along the c axis. Inset: Zoom in of the low- T data. The transitions at about 50 and 4.2 K correspond to the Morin transition of Fe^{3+} and the Néel transition of Dy^{3+} , respectively. The schematics illustrate the spin structures of Fe^{3+} (bottom, black) and Dy^{3+} (top, blue). (b) Anisotropic magnetization at $T = 2$ K. (c) Representative data of the low- T magnetic susceptibility in different magnetic fields along the c axis. Inset: field dependencies of the transition temperatures of the Dy^{3+} Néel order and the Fe^{3+} spin re-orientation, determined from the $M(T)$ curves.

be formed at a high temperature of $T_N^{\text{Fe}} \sim 645$ K, with a $G_x A_y F_z$ (Fe_I) spin configuration at room temperature. The transition at 50 K (T_M) is a Morin transition, where the Fe^{3+} structure changes to $A_x G_y C_z$ (Fe_{II}).²² Another transition at 4.2 K (T_N^{Dy}) corresponds to the AF ordering of Dy^{3+} moments in the $G_x A_y$ configuration. The low- T $M(H)$ curves shown in Fig. 1(b) are consistent with these spin structures.

When the field is applied along the c axis, the transition from Fe_I to Fe_{II} shifts to lower temperature rapidly with increasing field, but the AF order of Dy^{3+} is robust against the field, as seen in Fig. 1(c). It is known that

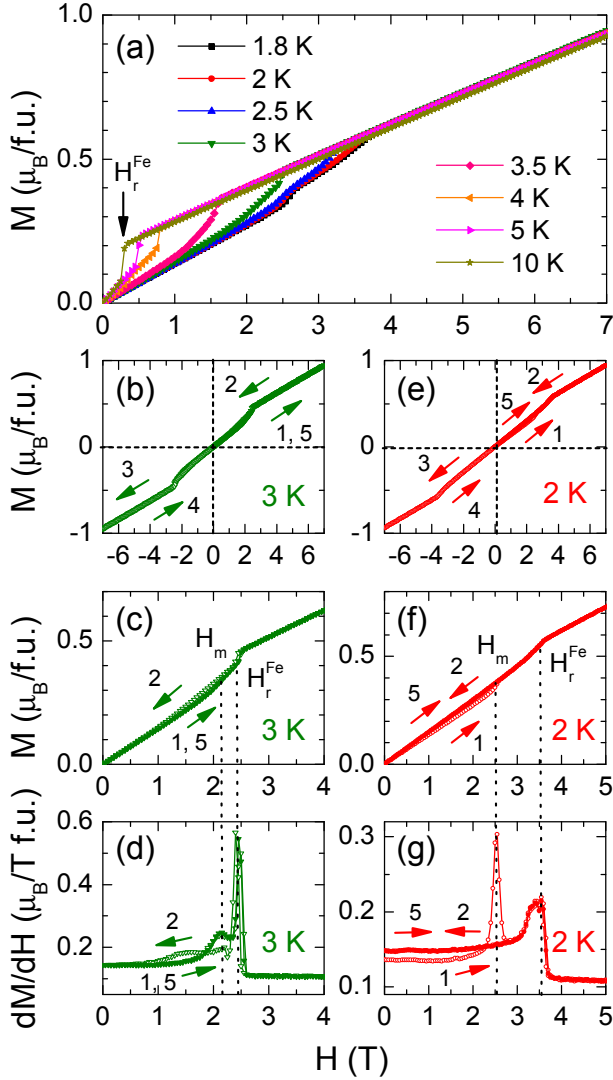


FIG. 2: (Color online) Magnetization of DyFeO₃ single crystal with $H \parallel c$ after ZFC. Panel (a) shows the magnetization in the positive field-up process. Other panels show full scan of magnetization between 7 and -7 T, the magnetization curves in the positive fields, and the differential curves with $T = 3$ K (b-d) and 2 K (e-g). The numbers and arrows denote the sweeping-field sequences and directions. The open and solid symbols denote the magnetization in the first full scan and the field-up process for the second time. H_r^{Fe} and H_m represent two transition fields, indicated by the peaks of the differential curves.

Dy³⁺ moments have strong anisotropy and are confined in the ab plane; therefore, the c -axis field can hardly to change either the Néel transition or the Dy³⁺ spin orientation. Thus, the irreversible $M(H)$, $P(H)$, and $\kappa(H)$ behaviors at low temperatures shown in the following sections are unambiguously related to the successive magnetic transitions of Fe³⁺ spins.

Figure 2 shows the magnetization of DyFeO₃ single crystal with $H \parallel c$ after ZFC. With $T > T_N^{\text{Dy}}$, M exhibits an abrupt increase at H_r^{Fe} , which corresponds to the spin-

flop transition of Fe³⁺ moments from Fe_{II} to Fe_I.^{8,24} With decreasing temperature, this transition gradually moves to higher field but becomes weaker, and finally evolves into a change of the slope (Fig. 2(a)). With $T < T_N^{\text{Dy}}$, there is a lower-field transition shown by a peak at H_m in the differential dM/dH curves, besides the peak at H_r^{Fe} , as shown in Figs. 2(d) and 2(g). Moreover, a peculiar irreversible $M(H)$ behavior is observed at $H < H_r^{\text{Fe}}$, with the irreversibility field slightly larger than H_m , as shown in Figs. 2(b-g). Note that this irreversibility is repeatable at $T > 2$ K (Figs. 2(c) and 2(d)), which means that the field-up M for the second time (solid symbol, label 5) is identical to that for the first field-up process (open symbol, label 1). However, with $T \leq 2$ K, the irreversibility becomes unrepeatable (Figs. 2(f) and 2(g)); that is, the field-up M for the second time is equal to that in the field-down process (open symbol, label 2). Therefore, there are two transitions in the field-up process and only the higher-field one exists when the field is swept down.

B. Electric Polarization

The electric polarization along the c axis of DyFeO₃ single crystal is measured down to subKelvin temperatures. Figure 3(a) shows the temperature dependencies of P measured after ME cooling from 5 K to 0.3 K with magnetic field and $E = 3$ kV/cm along the c axis. P is temperature independent at very low temperatures and decreases to zero at around T_N^{Dy} , which indicates that the Dy³⁺ spin order contributes to this electric polarization. The magnitude of P is enhanced and the transition temperature is slightly suppressed with increasing field. Figures 3(b-e) shows the magnetic-field dependence of P , measured after ME poling from 5 K in 7 T magnetic field and $E = 3$ kV/cm along the c axis. At low fields, $P(H)$ shows a linear ME behavior. With increasing field, the spin-flop transition of Fe³⁺ from Fe_{II} to Fe_I causes a change of the slope of $P(H)$ at $H = H_r^{\text{Fe}}$, and the multiferroicity shows up. These results are also in good agreement with the earlier work.⁸

However, $P(H)$ obtained with the ZFC process (cooling in zero magnetic field and electric field) shows very different behavior (Figs. 4(b-d)). First, the magnitude of P after ZFC is one or two orders smaller than that after ME poling, which is mainly due to the electric domains. Second and more importantly, an irreversible $P(H)$ is observed in the linear ME phase. At $T = 2$ K (Fig. 4(b)), for example, P is zero in low fields and exhibits a step-like increase at $H_m \approx 2.5$ T for the first field-up process. In higher-field, $P(H)$ is reversible and linear with field. Note that H_m increases with decreasing temperature and approaches H_r^{Fe} at 0.7 K (Figs. 4(b-d)). When $H > H_r^{\text{Fe}}$ (≈ 3.5 T), the system enters the multiferroic phase due to the spin-flop transition of Fe³⁺ sublattice.⁸ The values of H_m and H_r^{Fe} observed from $P(H)$ are essentially consistent with those of $M(H)$. This consistency suggests a

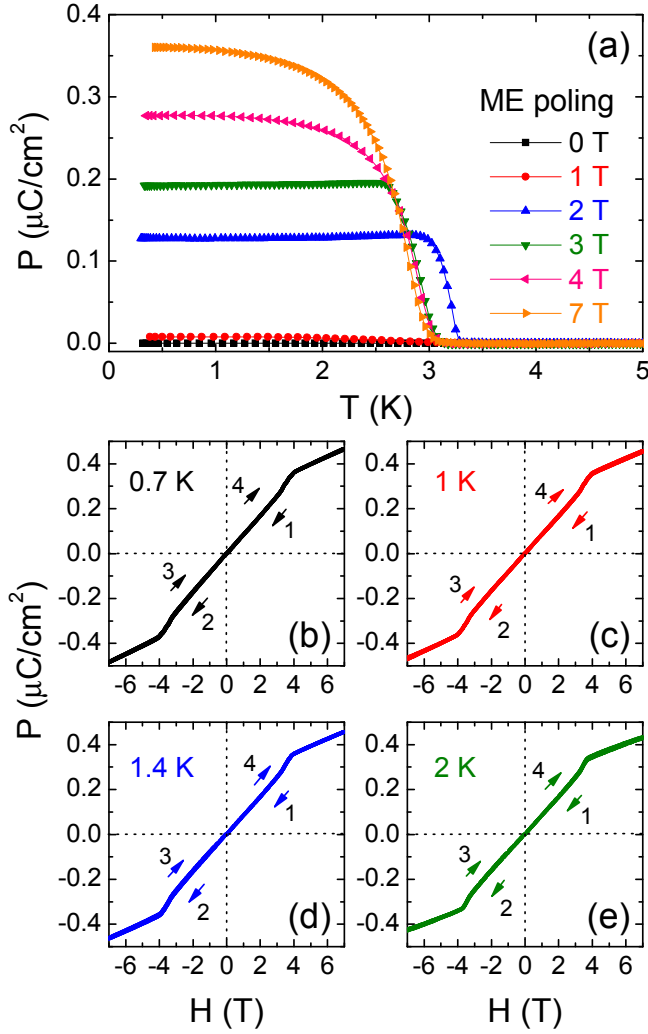


FIG. 3: (Color online) (a) Temperature dependencies of the c -axis electric polarization of DyFeO₃ single crystal measured after ME poling in magnetic field and $E = 3$ kV/cm electric field, both along the c axis. (b-e) Magnetic field dependencies of P measured after ME poling in 7 T and $E = 3$ kV/cm. The numbers and arrows denote the sweeping-field sequences and directions.

common origin for the observed irreversibility of $M(H)$ and $P(H)$.

C. Thermal Conductivity

The thermal conductivity of DyFeO₃ single crystal is studied for probing the magnetic transitions at even lower temperatures than our $M(H)$ and $P(H)$ measurements cannot be done.

Before presenting the heat transport results of DyFeO₃ crystal, we show in Fig. 5(a) the low- T specific heat data. A large and sharp peak is observed at 4.1 K, which is related to the Néel transition of Dy³⁺ spins. It can be seen that the magnetic contributions to the specific heat are

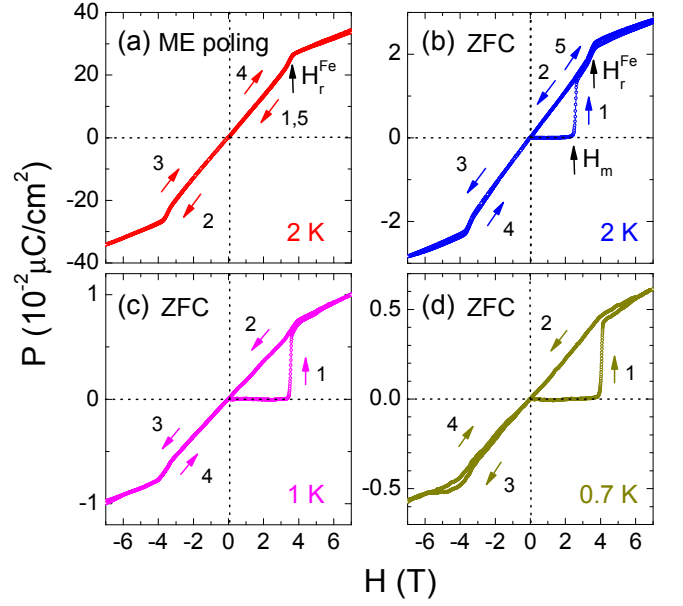


FIG. 4: (Color online) Magnetic-field dependencies of the electric polarization of DyFeO₃ single crystal measured at (a) 2 K after ME poling and (b-d) at 2 – 0.7 K after ZFC in $H \parallel c$. The numbers and arrows denote the sweeping-field sequences and directions. In panels (a) and (b), H_m and H_r^{Fe} indicates two transition fields and are the same as those from the magnetization.

important only at very low temperatures and are likely to be negligible above ~ 12 K, where the specific heat data show a minimum. Therefore, the phonon specific heat can be estimated from the high- T data in Fig. 5(a). It is known that in the temperature range $0.02 < T/\theta_D < 0.1$ (θ_D is the Debye temperature), the phonon specific heat follows a low-frequency expansion of the Debye function, $C = \beta T^3 + \beta_5 T^5 + \beta_7 T^7 + \dots$, where β , β_5 and β_7 are temperature-independent coefficients.³⁹ It is found that this formula fits well to the experimental data at $T > 15$ K, as shown in Fig. 5(a), with the fitting parameters $\beta = 1.28 \times 10^{-4}$ J/K⁴mol, $\beta_5 = 2.49 \times 10^{-7}$ J/K⁶mol and $\beta_7 = -1.75 \times 10^{-10}$ J/K⁸mol.

Figure 5(b) shows the temperature dependencies of the thermal conductivity down to 70 mK in zero field, with the heat current J_H applied along the c axis. For comparison, the data for YFeO₃ single crystal are also taken in the same temperature regime. Note that the Y³⁺ ions are nonmagnetic and there is only AF order of Fe³⁺ ions. YFeO₃ actually shows a simple and pure phonon heat transport phenomenon at low temperatures: (i) the $\kappa(T)$ curve exhibits a very large peak at about 20 K, with the peak value of 520 W/Km, indicating a very high quality of the single crystal; (ii) the temperature dependence of κ is roughly $T^{2.7}$ at subKelvin temperatures, which is close to the T^3 boundary scattering limit of phonons.³⁸ The DyFeO₃ data are rather comparable to those of YFeO₃, except for two notable differences. At first, the κ of DyFeO₃ is smaller at high tempera-

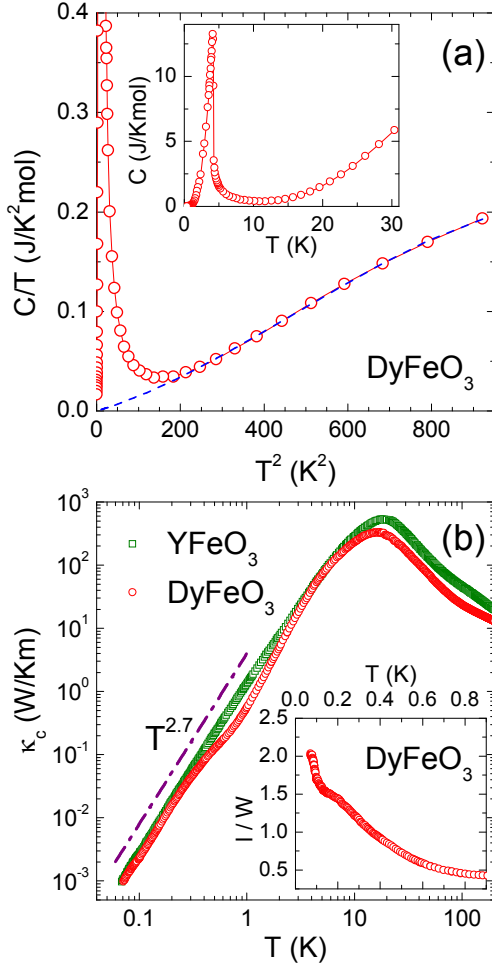


FIG. 5: (Color online) (a) The specific heat of DyFeO₃ single crystal below 30 K, plotted in C/T vs T^2 . The inset displays all the data at $T \leq 30$ K, which show a sharp peak at 4.1 K. The dashed line shows the fitting to the high- T data by using the formula of phonon specific heat, that is, $C = \beta T^3 + \beta_5 T^5 + \beta_7 T^7$. (b) Zero-field thermal conductivity of DyFeO₃ with heat current along the c axis. For comparison, the data of YFeO₃ is also presented. The sample sizes are $3.86 \times 0.63 \times 0.14$ mm³ and $4.40 \times 0.66 \times 0.16$ mm³ for DyFeO₃ and YFeO₃, respectively. The dash-dot line indicates a $T^{2.7}$ temperature dependence. The inset shows the temperature dependence of the phonon mean free path l divided by the averaged sample width W .

tures, although a phonon peak of 330 W/Km is also exceptionally larger for transition-metal oxides. More remarkably, there is a clear concave structure in the $\kappa(T)$ curve in the temperature regime of 0.3–3 K. A similar result has been found in another orthoferrite GdFeO₃.³² It is clear that at $T < T_N^{\text{Dy}}$, the magnon excitations from the Dy³⁺ spin system can have a significant scattering on phonons, which results in a downward deviation from the $T^{2.7}$ behavior. However, with lowering temperature further, the κ recovers to the $T^{2.7}$ dependence at $T < 300$ mK. This means that the magnon scattering effect is gradually smeared out. Apparently, the magnon spectra

has a finite energy gap (for example, originated from the spin anisotropy), which prevents the low-energy magnons from being thermally excited at very low temperatures.

It is possible to estimate the mean free path of phonons at low temperatures and to judge whether the phonons are free from microscopic scattering at subKelvin temperatures. The phononic thermal conductivity can be expressed by the kinetic formula $\kappa_{ph} = \frac{1}{3} C v_p l$,³⁸ where $C = \beta T^3$ is the phonon specific heat at low temperatures, v_p is the average velocity and l is the mean free path of phonons. Using the β value obtained from the above specific-heat data, the phonon velocity can be calculated and then the mean free path is obtained from the κ .^{32,33} The inset to Fig. 5(b) shows the ratio between l and the averaged sample width $W = 2\sqrt{A/\pi} = 0.335$ mm,^{32,33,38} where A is the area of cross section. It can be seen that l/W increases with lowering temperature and becomes larger than one at lowest temperatures, which indicates that all the microscopic phonon scatterings (including magnon scattering) are negligible and the boundary scattering limit is established.³⁸

The field dependence of thermal conductivity after ZFC is measured down to 92 mK and the results are presented in Fig. 6. With decreasing temperature, κ exhibits complicated field dependence: (i) with $T > 2$ K, $\kappa(H)$ is reversible and shows a sharp decrease at H_r^{Fe} ; (ii) with $0.7 \text{ K} \leq T \leq 2 \text{ K}$, $\kappa(H)$ shows an analogous irreversible behaviors to those of $M(H)$ and $P(H)$. There are two maximums in the field-up process and only the high-field one is kept when decreasing field, resulting in a larger κ in the field-down process at low fields; (iii) when temperature is further decreased down to below 500 mK, $\kappa(H)$ exhibits a different irreversible behavior; that is, there is only one dip in the sweeping-field run with a higher location in the field-up process. One notable feature is that the κ in the field-up process becomes larger than that in the field-down process, which is opposite to the case above 500 mK.

It has been known from many previous studies on the antiferromagnetic materials that the thermal conductivity could exhibit drastic changes at the magnetic phase transitions or the spin re-orientations.^{28–35} The mechanisms are mostly due to the sudden changes in the population of the magnetic excitations, which can effectively scatter phonons.^{31–35} In some rare case, the magnons well populated at the spin-flop transition can also contribute to the heat transport by acting as heat carriers.³³ In present work, the anomalies of the $\kappa(H)$ curves can be apparently attributed to the transitions of magnetic structures of DyFeO₃, which is also a common phenomenon to GdFeO₃.³² However, the hysteresis of $\kappa(H)$ are rather different between these two materials.

D. Phase Diagram and Magnetic Transitions

Considering the above experimental results, one can find a common feature for the ZFC $M(H)$, $P(H)$, and

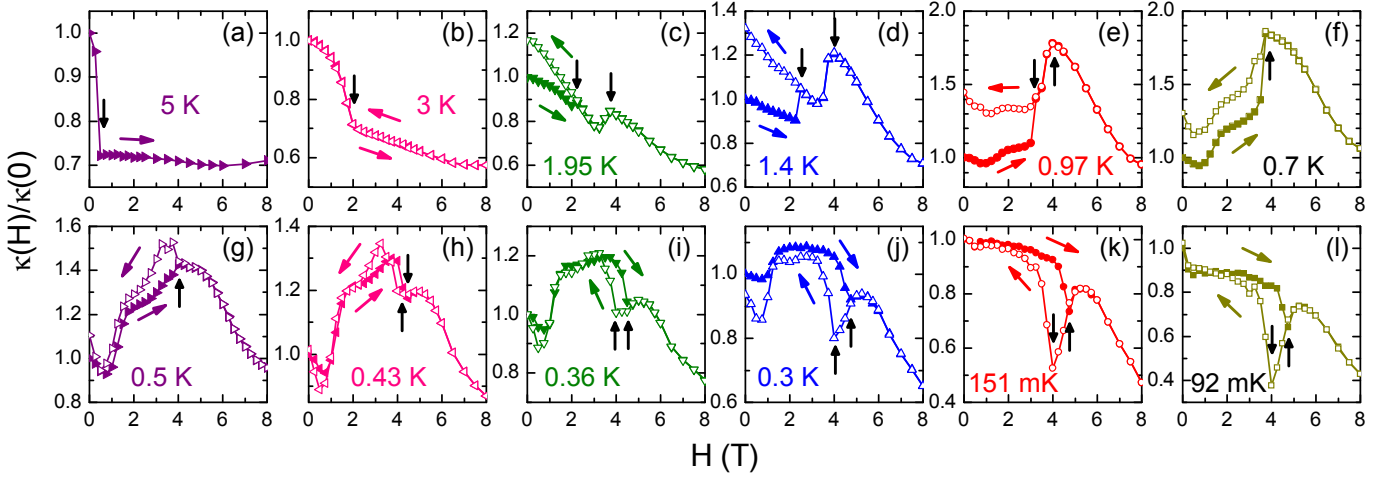


FIG. 6: (Color online) Magnetic-field dependencies of the c -axis thermal conductivity of DyFeO₃ single crystal in $H \parallel c$ after ZFC. As indicated by the colored arrows, the data shown with solid symbols are measured in the field-up process, while the open symbols show the data in the field-down process. The black upright arrows indicate the characteristic fields in $\kappa(H)$ isotherms.

$\kappa(H)$ data, that is, an irreversible behavior is observed only in the first field-up process, and it disappears in the following sweeping-field process. One possible reason for the observed irreversibility is the multi-domain effect in the multiferroic materials.⁹ Since the crystal is cooled in zero field without ME poling, at zero and low fields, the macroscopic polarization might be zero due to the compensation among different electric domains. With increasing field, the sample gradually changes into a fewer-domain state and the finite magnitude of P appears, which could be accompanied with some change in the $M(H)$ curve. However, from our results at $T \leq 2$ K, the $P(H)$ and $M(H)$ curves are reversible in the subsequent sweeping-field process except for the first one. This is obviously different from the case of the $P(H)/M(H)$ loop in usual ferroelectric/ferromagnetic materials, in which the loop always exists due to the presence of domains. On the other hand, if the domain effect is the major reason for the observed irreversibility, the phonon scattering by the domain walls should be effective in the whole low- T range. In the case of GdFeO₃,⁹ when the crystal is cooled in zero field, the field-up P is larger than that in the field-down run, which indicates that there are less ferroelectric domains with increasing field. The larger $\kappa(H)$ in the field-up process can be attributed to the weak phonon scattering by the domain walls.³² Similar to the case of GdFeO₃, the $\kappa(H)$ at $T > 500$ mK behaves consistently with the $M(H)$ and $P(H)$ curves in DyFeO₃; that is, the ME domain walls are likely playing a role in scattering phonons. However, upon further cooling (≤ 300 mK) the κ in the field-up process becomes larger than that in the field-down process, which can not be explained by the domain wall scattering on phonons. In a word, although the multi-domain effect could have influence on the magnitudes of $M(H)$, $P(H)$, and $\kappa(H)$, when the crystal is cooled without ME poling, it seems to

be not the dominant factor for the observed irreversible behaviors.

The second possible reason for the step-like increase of P and the consistent low-field irreversibility shown by $M(H)$, $P(H)$, and $\kappa(H)$ is the presence of an unknown zero-field magnetic structure below T_N^{Dy} after ZFC, which is metastable in the field and disappears when the field is swept down. Actually, it is a rather common feature of multiferroic materials that a metastable spin configuration is formed in ZFC process while another spin structure is stabilized after ME cooling. A recent example is the field-induced metastable phase in hexaferrites, observed by a neutron scattering.⁴⁰ This scenario can easily explain the $P(H)$ and $M(H)$ behaviors. Due to the strong out-of-plane anisotropy of Dy³⁺ spins, the applied field along the c axis could not change their spin arrangements directly, as the magnetization in Fig. 1(c) indicated. Most likely, only the change of Fe³⁺ spin structure is involved. Therefore, the zero-field structure of Fe³⁺ at $T < T_N^{\text{Dy}}$ should be different from the known Fe_{II} at $T > T_N^{\text{Dy}}$ and is hereafter named as Fe_{III}. It is also notable that the repeatable irreversibility begins to appear with $T < T_N^{\text{Dy}}$ and becomes unrepeatable with $T \leq 2$ K, the transition from Fe_{II} to Fe_{III} is therefore a gradual process between T_N^{Dy} and 2 K. Another notable feature is that the transition from Fe_{II} to Fe_I at $T > T_N^{\text{Dy}}$ could cause a sharp increase of M . Due to the presence of irreversibility, this feature gradually vanishes at $T < T_N^{\text{Dy}}$; instead, two successive magnetic transitions are present, and the higher-field one is from Fe_{II} to Fe_I, which is the same as the case at high temperatures.

Based on the above discussions and experimental data of $M(H)$, $P(H)$, and $\kappa(H)$, a low temperature $H - T$ phase diagram with $H \parallel c$ and in the case of ZFC is constructed, as shown in Fig. 7. We propose that be-

sides the known Fe_I and Fe_II , the phase diagram involves another magnetic phase, Fe_III . The most important feature is that the Fe^{3+} spins undergo successive transitions: $\text{Fe}_\text{III} \rightarrow \text{Fe}_\text{II} \rightarrow \text{Fe}_\text{I}$ with increasing field and at $500 \text{ mK} < T < T_\text{N}^{\text{Dy}}$, and only the transition from $\text{Fe}_\text{I} \rightarrow \text{Fe}_\text{II}$ is present when the field is decreased, which is consistent with the FC results. It is known that there are four Fe^{3+} spin configurations that could produce linear ME response, i.e., $G_x A_y F_z$ (Fe_I), $A_x G_y C_z$ (Fe_II), $F_x C_y G_z$, and $C_x F_y A_z$.³⁷ Since the crystal is cooled without ME poling, it is in principal difficult to judge from the electric polarization whether there is spontaneous P or not in zero field, and accordingly to judge the definite magnetic structure of Fe_III . This is because that the sample after ZFC could be in a multi-domain phase with spontaneous polarization, even though the measured P is zero. However, since the low- T $P(H)$ loops actually behave rather differently from the usual $P(H)$ hysteresis curves, some kind of magnetic-structure transition other than the multi-domain effect may play a more important role. Nevertheless, we have to leave the definition of the Fe_III magnetic structure as an open question, and further investigations like neutron scattering studies on single crystals are called for.

This phase diagram could explain the behavior of $\kappa(H)$ down to the lowest temperature. (i) With $T > T_\text{N}^{\text{Dy}}$, when the field is applied, the Fe^{3+} spin structure changes from Fe_II to Fe_I . Accordingly, a sharp decrease of κ is observed, due to the phonon scattering by the magnetic excitations.^{31,32,34} (ii) With $T \leq 2 \text{ K}$, the applied field could induce successive transitions from Fe_III to Fe_II and then to Fe_I in the field-up process, and $\kappa(H)$ shows two local maximums due to the weakened scattering of phonons across each transition. The transition from Fe_II to Fe_III is absent when the field is decreased, resulting in a larger κ below H_m . (iii) With further cooling, H_m becomes larger and there is only a first-order transition from Fe_III to Fe_I directly with $T < 500 \text{ mK}$, which results in a different field dependence of κ . It should be noted that below 500 mK the Fe_III state is always present in the sweeping-field process. This indicates that the Fe_III state, which is metastable in sweeping magnetic field above 500 mK , becomes stable at $T < 500 \text{ mK}$.

In passing, it should be pointed out that, besides the magnon excitations, the paramagnetic spins could also have influence on the phonon thermal conductivity.^{38,41,42} Due to the paramagnetic scattering effect, $\kappa(H)$ usually shows a dip-like behavior. From Figs. 6(e-j), the dip around 1 T may be ascribed to the paramagnetic scattering on phonons. The complicated field dependencies at low fields between 0.97 K and 300 mK could be regarded as a superposition of magnon scattering at H_m on the recovery of κ due to the paramagnetic scattering, as indicated by the shoulder-like feature around 2 T for both field-up and field-down processes.

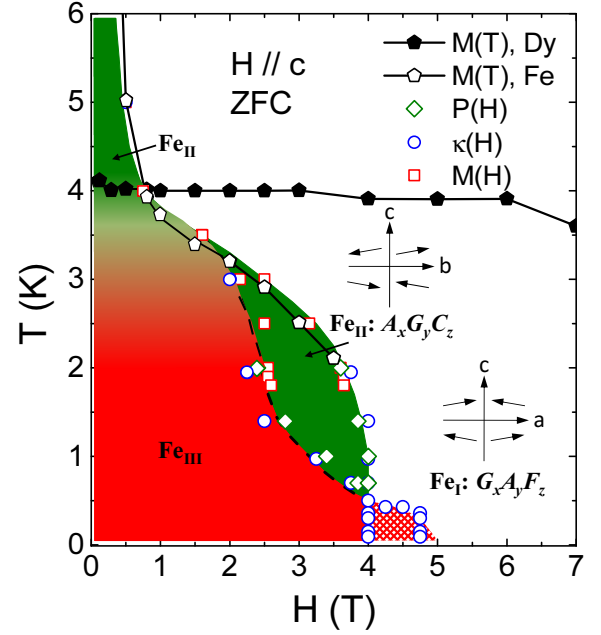


FIG. 7: (Color online) ZFC $H - T$ phase diagram of DyFeO_3 obtained from the $M(H)$, $P(H)$, and $\kappa(H)$ data. The transition from Fe_II to Fe_III is actually a gradual change, as a continuous change of color indicates. Above 500 mK , Fe_III is a metastable state; that is, it exits when sweeping-up field to the boundary indicated by the dashed line but does not appear when sweeping-down field. Below 500 mK , Fe_III becomes stable in sweeping field. The crossed red area represents an irreversible region due to the first-order transition from Fe_III to Fe_I . The transition temperatures of the Néel order and the spin re-orientation for Dy^{3+} and Fe^{3+} , determined from the $M(T)$ curves (Fig. 1(c)), are also shown.

IV. SUMMARY

Our detailed results of magnetization, electric polarization, and thermal conductivity point to a complex magnetic phase diagram of DyFeO_3 involving successive field-induced magnetic phase transitions of Fe^{3+} spins. First, the unknown ground state at ultra-low temperatures (Fe_III) is likely to have no linear ME effect. Apparently, this ground state is determined by the interaction between Dy^{3+} and Fe^{3+} spins. In particular, when the Dy^{3+} sublattice orders antiferromagnetically at T_N^{Dy} , the Fe^{3+} spins have to change their orientation. Second, with $500 \text{ mK} < T \leq 2 \text{ K}$, a low-field irreversibility of the magnetic transitions is observed when the sample is cooled in zero field, which indicates that Fe_III structure is metastable with sweeping magnetic field. A similar irreversible behavior is probably the one found in another orthoferrite TbFeO_3 , probed by the capacitance measurement,⁴³ in which an unknown low-field phase also disappeared with sweeping-down field. It seems that only at very low temperatures ($< 500 \text{ mK}$), the interaction between Dy^{3+} and Fe^{3+} spins is strong enough to stabilize the Fe_III structure. The further studies of these mate-

rials and probably other members of orthoferrite $R\text{FeO}_3$ could help to explore their complicated low- T magnetic structures and related interesting ME effect.

Acknowledgments

This work was supported by the National Natural Science Foundation of China, the National Basic Re-

search Program of China (Grants No. 2009CB929502, 2011CBA00111, and 2012CB922003), and the Fundamental Research Funds for the Central Universities (Programs No. WK2340000035 and WK2030220014).

-
- * Electronic address: xiazhao@ustc.edu.cn
† Electronic address: xfsun@ustc.edu.cn
- ¹ B. Lake, K. Lefmann, N. B. Christensen, G. Aeppli, D. F. McMorrow, H. M. Ronnow, P. Vorderwisch, P. Smeibidl, N. Mankorntong, T. Sasawa, M. Nohara, and H. Takagi, *Nature Mater.* **4**, 658 (2005).
 - ² H. J. Kang, P. Dai, J. W. Lynn, M. Matsuura, J. R. Thompson, S.-C. Zhang, D. N. Argyriouk, Y. Onose, and Y. Tokura, *Nature* **423**, 522 (2003).
 - ³ H. Pfau, S. Hartmann, U. Stockert, P. Sun, S. Lausberg, M. Brando, S. Friedemann, C. Krellner, C. Geibel, S. Wirth, S. Kirchner, E. Abrahams, Q. Si, and F. Steglich, *Nature* **484**, 493 (2012).
 - ⁴ T. Kimura, T. Goto, H. Shintani, K. Ishizaka, T. Arima, and Y. Tokura, *Nature* **426**, 55 (2003).
 - ⁵ H. Katsura, N. Nagaosa, and A. V. Balatsky, *Phys. Rev. Lett.* **95**, 057205 (2005).
 - ⁶ T. Goto, T. Kimura, G. Lawes, A. P. Ramirez, and Y. Tokura, *Phys. Rev. Lett.* **92**, 257201 (2004).
 - ⁷ T. Kimura, G. Lawes, T. Goto, Y. Tokura, and A. P. Ramirez, *Phys. Rev. B* **71**, 224425 (2005).
 - ⁸ Y. Tokunaga, S. Iguchi, T. Arima, and Y. Tokura, *Phys. Rev. Lett.* **101**, 097205 (2008).
 - ⁹ Y. Tokunaga, N. Furukawa, H. Sakai, Y. Taguchi, T. Arima, and Y. Tokura, *Nature Mater.* **8**, 558 (2009).
 - ¹⁰ J.-H. Lee, Y. K. Jeong, J. H. Park, M.-A. Oak, H. M. Jang, J. Y. Son, and J. F. Scott, *Phys. Rev. Lett.* **107**, 117201 (2011).
 - ¹¹ Y. J. Choi, H. T. Yi, S. Lee, Q. Huang, V. Kiryukhin, and S.-W. Cheong, *Phys. Rev. Lett.* **100**, 047601 (2008).
 - ¹² D. Higashiyama, S. Miyasaka, and Y. Tokura, *Phys. Rev. B* **72**, 064421 (2005).
 - ¹³ M. Fukunaga, Y. Sakamoto, H. Kimura, Y. Noda, N. Abe, K. Taniguchi, T. Arima, S. Wakimoto, M. Takeda, K. Kakurai, and K. Kohn, *Phys. Rev. Lett.* **103**, 077204 (2009).
 - ¹⁴ D. Higashiyama, S. Miyasaka, N. Kida, T. Arima, and Y. Tokura, *Phys. Rev. B* **70**, 174405 (2004).
 - ¹⁵ A. V. Kimel, A. Kirilyuk, A. Tsvetkov, R. V. Pisarev, and T. Rasing, *Nature* **429**, 850 (2004).
 - ¹⁶ A. V. Kimel, A. Kirilyuk, P. A. Usachev, R. V. Pisarev, A. M. Balbashov, and T. Rasing, *Nature* **435**, 655 (2005).
 - ¹⁷ A. V. Kimel, B. A. Ivanov, R. V. Pisarev, P. A. Usachev, A. Kirilyuk, and T. Rasing, *Nature Phys.* **5**, 727 (2009).
 - ¹⁸ Y. Tokunaga, Y. Taguchi, T. Arima, and Y. Tokura, *Nature Phys.* **8**, 838 (2012).
 - ¹⁹ K. Yamaguchi, T. Kurihara, Y. Minami, M. Nakajima, and T. Suemoto, *Phys. Rev. Lett.* **110**, 137204 (2013).
 - ²⁰ E. F. Bertaut, *Magnetism*, Vol. 3, (Academic Press, New York, 1963).
 - ²¹ A. Berton and B. Sharon, *J. Appl. Phys.* **39**, 1367 (1968).
 - ²² G. Gorodetsky, B. Sharon, and S. Shtrikman, *J. Appl. Phys.* **39**, 1371 (1968).
 - ²³ F. J. Morin, *Phys. Rev.* **78**, 819 (1950).
 - ²⁴ L. A. Prelorendjo, C. E. Johnson, M. F. Thomas, and B. M. Wanklyn, *J. Phys. C: Solid Stat. Phys.* **13**, 2567 (1980).
 - ²⁵ L. M. Holmes, L. G. Van Uitert, R. R. Hecker, and G. W. Hull, *Phys. Rev. B* **5**, 138 (1972).
 - ²⁶ L. M. Holmes and L. G. Van Uitert, *Phys. Rev. B* **5**, 147 (1972).
 - ²⁷ M. Belakhovsky, M. Bogé, J. Chappert, and J. Sivardière, *Solid State Commun.* **20**, 473 (1976).
 - ²⁸ A. V. Sologubenko, K. Berggold, T. Lorenz, A. Rosch, E. Shimshoni, M. D. Phillips, and M. M. Turnbull, *Phys. Rev. Lett.* **98**, 107201 (2007).
 - ²⁹ A. V. Sologubenko, T. Lorenz, J. A. Mydosh, A. Rosch, K. C. Shortsleeves, and M. M. Turnbull, *Phys. Rev. Lett.* **100**, 137202 (2008).
 - ³⁰ X. F. Sun, W. Tao, X. M. Wang, and C. Fan, *Phys. Rev. Lett.* **102**, 167202 (2009).
 - ³¹ X. M. Wang, C. Fan, Z. Y. Zhao, W. Tao, X. G. Liu, W. P. Ke, X. Zhao, and X. F. Sun, *Phys. Rev. B* **82**, 094405 (2010).
 - ³² Z. Y. Zhao, X. M. Wang, C. Fan, W. Tao, X. G. Liu, W. P. Ke, F. B. Zhang, X. Zhao, and X. F. Sun, *Phys. Rev. B* **83**, 014414 (2011); *ibid.* **89**, 099903(E) (2014).
 - ³³ Z. Y. Zhao, X. M. Wang, B. Ni, Q. J. Li, C. Fan, W. P. Ke, W. Tao, L. M. Chen, X. Zhao, and X. F. Sun, *Phys. Rev. B* **83**, 174518 (2011).
 - ³⁴ C. Fan, Z. Y. Zhao, H. D. Zhou, X. M. Wang, Q. J. Li, F. B. Zhang, X. Zhao, and X. F. Sun, *Phys. Rev. B* **87**, 144404 (2013).
 - ³⁵ F. B. Zhang, Q. J. Li, Z. Y. Zhao, C. Fan, S. J. Li, X. G. Liu, X. Zhao, and X. F. Sun, *Phys. Rev. B* **89**, 094403 (2014).
 - ³⁶ X. F. Sun, K. Segawa, and Y. Ando, *Phys. Rev. Lett.* **93**, 107001 (2004).
 - ³⁷ T. Yamaguchi and K. Tsushima, *Phys. Rev. B* **8**, 5187 (1973).
 - ³⁸ R. Berman, *Thermal Conduction in Solids* (Oxford University Press, Oxford, 1976).
 - ³⁹ A. Tari, *Specific Heat of Matter at Low Temperatures* (Imperial College Press, 2003).
 - ⁴⁰ H. B. Lee, Y.-S. Song, J.-H. Chung, S. H. Chun, Y. S. Chai, K. H. Kim, M. Reehuis, K. Prokeš, and S. Mat'áš, *Phys. Rev. B* **83**, 144425 (2011).
 - ⁴¹ X. F. Sun, I. Tsukada, T. Suzuki, S. Komiya, and Y. Ando, *Phys. Rev. B* **72**, 104501 (2005).
 - ⁴² X. F. Sun, A. A. Taskin, X. Zhao, A. N. Lavrov, and Y. Ando, *Phys. Rev. B* **77**, 054436 (2008).

⁴³ S. Artyukhin, M. Mostovoy, N. P. Jensen, D. Le, K. Prokes, V. G. de Paula, H. N. Bordallo, A. Maljuk, S. Landsgesell, H. Ryll, B. Klemke, S. Paeckel, K. Kiefer, K. Lefmann,

L. T. Kuhn, and D. N. Argyriou, *Nature Mater.* **11**, 694 (2012).